DTU Library

How the relative permittivity of solar cell materials influences solar cell performance

Crovetto, Andrea; Huss-Hansen, Mathias K.; Hansen, Ole

Link back to DTU Orbit

How the relative permittivity of solar cell materials influences solar cell performance

Andrea Crovetto[a,*], Mathias K. Huss-Hansen[a], Ole Hansen[a,b]

[a]*DTU Nanotech, Technical University of Denmark, DK-2800 Kgs. Lyngby, Denmark*
[b]*V-SUSTAIN, Villum Center for the Science of Sustainable Fuels and Chemicals, Technical University of Denmark, DK-2800 Kgs. Lyngby, Denmark*

Abstract

The relative permittivity of the materials constituting heterojunction solar cells is usually not considered as a design parameter when searching for novel combinations of heterojunction materials. In this work, we investigate whether such an approach is valid. Specifically, we show the effect of the materials permittivity on the physics and performance of the solar cell by means of numerical simulation supported by analytical relations. We demonstrate that, depending on the specific solar cell configuration and materials properties, there are scenarios where the relative permittivity has a major influence on the achievable conversion efficiency, and scenarios where its influence can be safely ignored. In particular, we argue that high-permittivity materials should always be the preferred choice as heterojunction partners of the absorber layer when prototyping new materials combinations. When the heterojunction partner has a high permittivity, solar cells are consistently more robust against several non-idealities that are especially likely to occur in early-stage development, when the device is not yet optimized.

Keywords:
permittivity, dielectric constant, heterojunction solar cell, device physics, CIGS

1. Introduction

Within the last few years, impressive power conversion efficiencies have been demonstrated by various heterojunction solar cell technologies. Si-based heterojunction intrinsic thin layer (HIT), CdTe, Cu(In,Ga)Se$_2$ (CIGS), and metal halide perovskite solar cells have all reached efficiencies above 20% [1] and can be manufactured at a relatively low cost. The earth-abundant and non-toxic absorber Cu$_2$ZnSn(S,Se)$_4$ (CZTS) has also been investigated extensively and has reached a promising 12.6% record efficiency [1].

Assuming a p-type absorber material, heterojunction solar cells typically feature a moderately doped thin layer (n-type), often called "buffer layer" or "intrinsic layer", as the immediate heterojunction partner of the absorber layer. This is followed by a layer with heavier doping (n$^+$-type), often called "window layer" or "electron transport layer". Such a solar cell architecture is shown in Fig. 1. Especially for CIGS and CZTS solar cells, there is an ongoing effort to replace the standard CdS buffer layer with another material [2]. The reasons are the toxicity of Cd and relatively low band gap of CdS (2.4 eV), which means that an appreciable fraction of light is absorbed in this layer, where carrier collection efficiency is low.

Selection of potential candidates as buffer layer materials is typically based on criteria such as 1) wide band gap, 2) natural occurrence of doping of opposite type as the absorber layer, 3) favorable conduction band offset with the absorber layer, 4) lattice matching with the absorber layer, 5) good coverage of the absorber layer, 6) absence of detrimental chemical interdiffusion with the absorber layer. While all the above reasons are valid, efficiency limitations arising from an unfavorable relative permittivity of the buffer layer have not been discussed in detail. In general, the relative permittivity $\varepsilon_r(\omega)$ of a material, also known as dielectric constant, depends on frequency ω or, equivalently, on photon energy. It describes how the material polarizes under the application of an electric field. For solar cell applications, two spectral regions are of primary interest. The first is the static permittivity $\varepsilon_r(0)$, or simply ε_r, which describes polarization under a constant electric field. This is a relevant quantity in the depletion region of a solar cell, where a constant electric field exists due to the presence of a space charge region [3]. The second important spectral region corresponds to the solar spectrum (optical frequencies). In this region, the relative permittivity becomes a complex number and describes the optical phenomena of light absorption and refraction in the solar cell material [4, 5]. Optical optimization of solar cells has already received much attention in solar cell research and will not be treated here. Instead, this work will focus on the static component of the permittivity while the optical component is kept fixed. The static component will be simply called "relative permittivity" or "permittivity" in the following for simplicity.

To study the effect of the materials permittivity on solar cell performance, we will use a generic absorber/buffer/window solar cell architecture inspired by CIGS solar cell technology. This approach follows the recommendation of a reference book on heterojunction solar cell design [6]. Throughout this work, we will present different scenarios in which the relative permittivity of the solar cell materials affects the power conversion efficiency significantly. We will show which physical mecha-

nisms are responsible for the observed changes in efficiency and we will quantify such changes by device simulation. Based on those results, we will suggest a design rule for the relative permittivity of novel heterojunction solar cell materials. The rule is relatively easy to implement since the relative permittivity of materials is usually known or easily measurable [7].

2. Theory

2.1. Effect on depletion region width

Using standard equations for p-n heterojunctions in the depletion approximation with a p-type absorber and an n-type partner, the effect of the relative permittivity of the two heterojunction materials on device operation can be summarized by two mathematical relations [3]. The first is

$$W = \left[\frac{2V_{bi}\varepsilon_n\varepsilon_p(N_d + N_a)^2}{eN_dN_a(\varepsilon_nN_d + \varepsilon_pN_a)} \right]^{1/2} \tag{1}$$

Here W is the total width of the depletion region, ε_n and ε_p are the static permittivites of the n- and p-type semiconductors, V_{bi} is the built-in voltage in equilibrium, e is the elementary charge and N_a and N_d are the acceptor and donor densities of the p- and n-type material, respectively (Fig. 1). In most practical cases, both light absorption and collection efficiency are low in the n-type heterojunction partner, so it can be more instructive to deal with the part of the depletion region that lies in the p-type absorber, which has a width

$$W_p = \left[\frac{2V_{bi}\varepsilon_n\varepsilon_pN_d}{eN_a(\varepsilon_nN_d + \varepsilon_pN_a)} \right]^{1/2} \tag{2}$$

Eq. 2 predicts that the width of the depletion region increases as the permittivity of the two heterojunction materials increases. Notice that, if one of the two sides of the junction is doped heavily with respect to the other, then it is only the permittivity of the lightly-doped side of the junction that contributes to depletion region widening. Since minority carriers are collected most efficiently within a depth corresponding to the depletion width in the absorber layer plus their diffusion length, widening of the depletion region increases the depth at which the carriers can be efficiently collected. This can noticeably increase the short circuit current density J_{sc} in the cases where the total width of the two above regions is not enough to efficiently collect all photo-generated carriers, especially those due to long-wavelength photons. If, on the contrary, the collection length is large compared to the light absorption depth in the absorber material, the short circuit current is unaffected by the permittivities. The influence of the permittivity on solar cell performance in those two scenarios will be shown in detail in Sec. 4.5.

2.2. Effect on built-in voltage distribution

The second relation [3] describing the effect of the materials permittivity on device performance is the following:

$$\frac{V_{bi,n}}{V_{bi,p}} = \frac{\varepsilon_pN_a}{\varepsilon_nN_d} \tag{3}$$
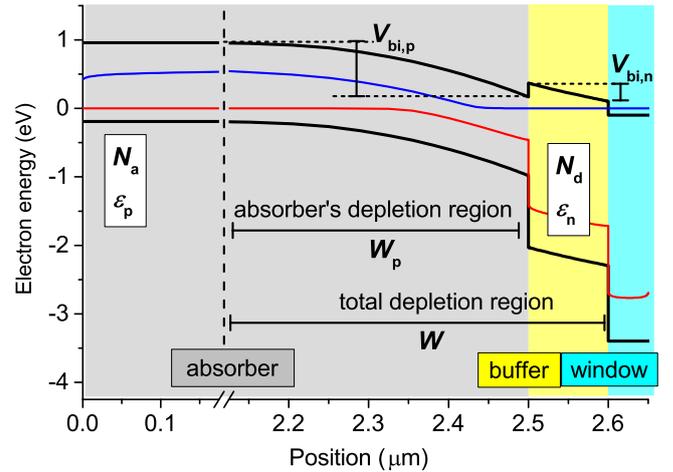

Figure 1: Simulated band diagram of the baseline solar cell used in this work, under standard AM 1.5 illumination and with no applied voltage. The case of the high-permittivity ratio is plotted (ε_p = 13.6 and ε_n = 20). The black lines are the valence- and conduction band edges. The blue (red) line is the quasi-Fermi level for electrons (holes) under illumination.

Here, $V_{bi,n}$ and $V_{bi,p}$ are the built-in voltage drops in the n-type and p-type junction materials, as shown in Fig. 1. This relation is valid for a single heterojunction without interface charge. If there is a high interface charge density the $V_{bi,n}/V_{bi,p}$ ratio is not determined by Eq. 3 anymore, but it is determined by the energy level of the charged state at the interface ("Fermi level pinning"). For intermediate cases with moderate interface charge density, no simple expression exists to calculate the $V_{bi,n}/V_{bi,p}$ ratio, which must therefore be determined by numerical simulation. This will be done in Sec. 4.3 and Sec. 4.4.

For an ideal heterointerface (i.e., with zero interface recombination velocity), the $V_{bi,n}/V_{bi,p}$ ratio does not affect the efficiency [6]. However, in the presence of interface recombination, an increase in the $V_{bi,n}/V_{bi,p}$ ratio leads to a decrease in the open circuit voltage V_{oc} (for $0 < V_{bi,n}/V_{bi,p} < 1$) and in the short circuit current J_{sc} (for $V_{bi,n}/V_{bi,p} > 1$), due to trends in the relative abundance of electrons and holes at the interface [6]. Hence, the $\varepsilon_n/\varepsilon_p$ ratio is a key quantity that can in principle be used to tune the built-in voltage drop distribution $V_{bi,n}/V_{bi,p}$ and therefore the efficiency of the solar cell. Specifically, it appears that increasing the $\varepsilon_n/\varepsilon_p$ ratio is beneficial for increasing solar cell efficiency. However, this statement must be qualified by several factors. First of all, if the n-type material is much more highly doped than the p-type material, $V_{bi,n}$ will be very small compared to $V_{bi,p}$ regardless of the permittivity ratio, as permittivities of most semiconductors only vary over one order of magnitude. This renders all buffer-free solar cell architectures – with the absorber in direct contact with a highly doped window – insensitive to the $\varepsilon_n/\varepsilon_p$ ratio. On the other hand, if N_d is not much greater than N_a, then the permittivity ratio can significantly influence the voltage drop ratio, as will become evident in Sec. 4.1. However, even under those conditions, if the lowly-doped buffer layer is thin enough it will be completely depleted, such that $V_{bi,n}$ will be dictated solely by its doping

density and thickness, and not by its permittivity. This will also be shown numerically in Sec. 4.1. In the limiting case of an infinitely thin buffer layer, we are again in the case of a direct heterojunction discussed above. Finally, if interface charge is present in appreciable amount, Fermi level pinning occurs and Eq. 3 is again invalidated, because the built-in voltage drop distribution is now dictated by the (pinned) position of the Fermi level at the interface. Negative interface charge can be present in the form of occupied acceptor states (Sec. 4.4), which have a detrimental effect on V_{oc} because they increase $V_{bi,n}/V_{bi,p}$. On the other hand, unoccupied donor states close to the conduction band (positive interface charge, Sec. 4.3) have a beneficial effect on V_{oc} because they decrease $V_{bi,n}/V_{bi,p}$.

In Sec. 4, we will quantify variations in solar cell performance in the cases where the permittivity does play a role. From now on, the p and n subscripts of the discussed physical quantities always refer to the absorber and buffer layers respectively. This is because the window layer used in the model does not contribute to any built-in voltage drop due to its higher doping density (about two orders of magnitude higher than the absorber and the buffer, see Table 1).

3. Simulation details

Device-level simulations were performed numerically in one dimension with the finite-element method as implemented in the thin-film solar cell simulation software SCAPS [8]. The simulated solar cell has the absorber/buffer/window architecture and its simulated band diagram is shown in Fig. 1. The actual materials parameters, shown in Table 1, were taken from various literature sources [6, 9, 10] and are based on a CIGS absorber, a CdS buffer, and a ZnO window. This approach was also followed in [6] as a case study to formulate general design rules for heterojunction solar cells. We emphasize that we have tried to keep the solar cell model as simple as possible and we have purposely avoided simulating peculiar aspects of CIGS solar cells, such as band gap broadening at the heterointerface due to formation of the ordered vacancy compound [10, 11]. This is because our goal is to provide a reasonable baseline model to predict qualitatively how the permittivity influences the efficiency in a generic heterojunction solar cell, rather than to model a CIGS solar cell as accurately as possible. Except for the parameters varied in each simulation, and unless otherwise specified, the parameters used in all simulations are always fixed to their baseline values, which are specified in Table 1.

4. Results

To show how solar cell performance is sensitive to changes in the $\varepsilon_n/\varepsilon_p$ ratio, two cases are considered in each simulation. Case A (B) corresponds to a low (high) buffer-to-absorber permittivity ratio. In both cases, the permittivity of the absorber is fixed at $\varepsilon_p = 13.6$ as in a CIGS absorber [12]. In Case A (B), the permittivity of the buffer is set to $\varepsilon_n = 8$ ($\varepsilon_n = 20$), corresponding to ZnS and to CdO respectively [13, 14]. The permittivity of commonly used buffer layer materials falls within this range.

The permittivity ratio sensitivity factor Γ is then employed as a single indicator to summarize how solar cell performance is sensitive to changes in the $\varepsilon_n/\varepsilon_p$ ratio. Γ is defined as follows:

$$\Gamma = \frac{\eta_{\varepsilon_A}}{\eta_{\varepsilon_B}} \tag{4}$$

where η_{ε_A} is the simulated power conversion efficiency of the solar cell for Case A (low buffer-to-absorber permittivity ratio), and η_{ε_B} is the simulated efficiency for Case B (high buffer-to-absorber permittivity ratio). In short, if $\Gamma \sim 1$, the $\varepsilon_n/\varepsilon_p$ ratio does not affect the efficiency; if $\Gamma < 1$, the efficiency decreases as the $\varepsilon_n/\varepsilon_p$ ratio decreases.

In Figs. 2-5, we quantify variations in Γ due to the influence of the permittivity ratio $\varepsilon_n/\varepsilon_p$ on voltage drop ratio $V_{bi,n}/V_{bi,p}$ (Eq. 3 and Sec. 2.2). Those variations in Γ are primarily due to open circuit voltage variations as long as $V_{bi,n}/V_{bi,p}$ is not too large, as discussed in Sec. 2.2.

4.1. Dependence on buffer doping density and thickness

Fig. 2 demonstrates quantitatively what was qualitatively discussed in Sec. 2.2, i.e., that in the limit of high buffer doping or small buffer thickness, the efficiency is independent of the $\varepsilon_n/\varepsilon_p$ ratio. For high buffer doping, this occurs because $V_{bi,n}$ remains small even in the case of a high $\varepsilon_n/\varepsilon_p$ ratio. For a thin buffer with low doping, on the other hand, this occurs because the buffer is completely depleted regardless of the permittivity ratio, and therefore $V_{bi,n}$ is determined only by the donor doping density and buffer thickness.

This simulation demonstrates that a high $\varepsilon_n/\varepsilon_p$ ratio helps maintain a reasonably high efficiency even in solar cells with a thick and/or weakly doped buffer layer.

4.2. Dependence on heterointerface quality

In Fig. 3, we analyze the effect of interface quality on Γ. By conduction band offset, we intend the conduction band discontinuity at the heterointerface. In our model, the offset is equal to the difference in electron affinity between the absorber and the buffer. As discussed in Sec. 2.2, increasing interface recombination velocity increases the severity of the losses related to the potential drop $V_{bi,n}$ in the buffer, and Γ decreases accordingly due to Eq. 3. This effect becomes more severe as the conduction band offset decreases, because the device becomes more sensitive to the $V_{bi,n}/V_{bi,p}$ ratio [6, 9].

This simulation demonstrates that a high $\varepsilon_n/\varepsilon_p$ ratio alleviates the efficiency losses related to non-idealities at the heterointerface, such as unfavorable band alignment and high interface recombination velocity.

4.3. Dependence on interface donor states

In Fig. 4, we examine the influence of Fermi level pinning on Γ. While keeping the (neutral) interface defects responsible for the baseline interface recombination velocity as in the above studies, we add a single interface donor state with different densities and at different energy levels. If the interface donors are sufficiently abundant and sufficiently close to the conduction band, the interface Fermi level is pinned to the donor level, the
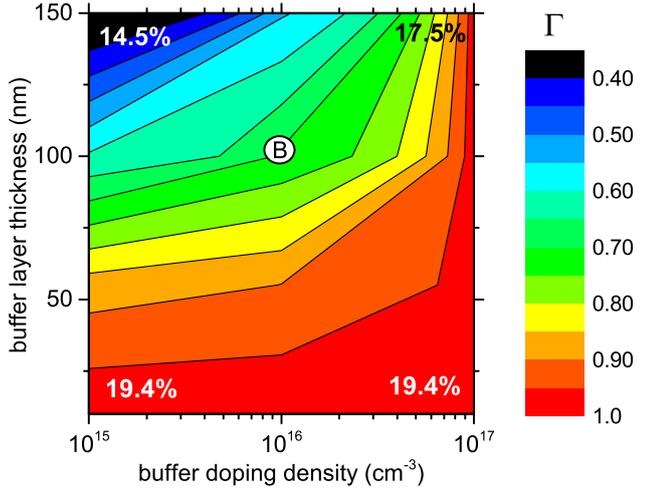
Figure 2: The effect of buffer layer thickness and doping level on the permittivity ratio sensitivity factor Γ. The circle with the "B" label indicates the baseline parameters. The overlaid numbers are the values of η_{ε_B}, i.e. the solar cell efficiency with a high buffer-to-absorber permittivity ratio, at the corresponding point in the parameter space.
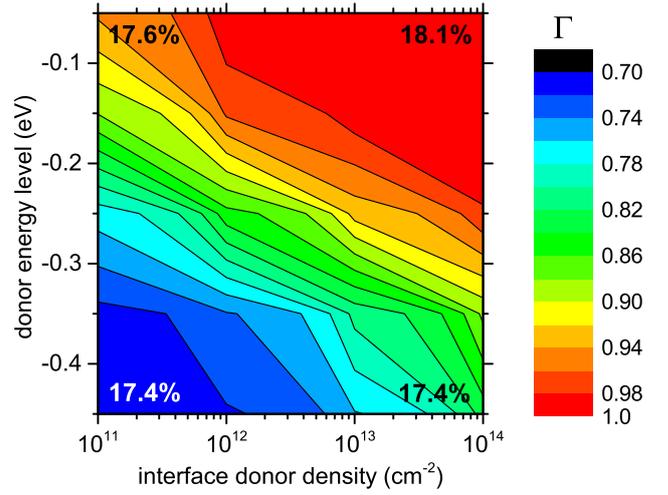

Figure 4: The effect of absorber-buffer interface donor density and energy level (referenced to the conduction band of the absorber layer) on the permittivity ratio sensitivity factor Γ. The overlaid numbers are the values of η_{ε_B}, i.e. the solar cell efficiency with a high buffer-to-absorber permittivity ratio, at the corresponding point in the parameter space.
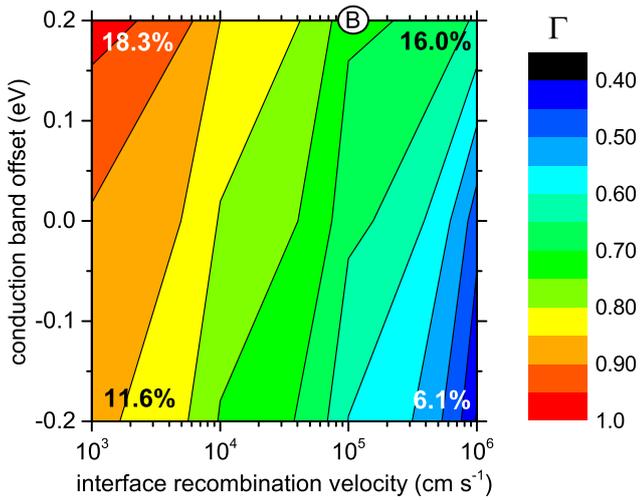

Figure 3: The effect of absorber-buffer interface recombination velocity and absorber-buffer conduction band offset on the permittivity ratio sensitivity factor Γ. The circle with the "B" label indicates the baseline parameters. The overlaid numbers are the values of η_{ε_B}, i.e. the solar cell efficiency with a high buffer-to-absorber permittivity ratio, at the corresponding point in the parameter space.
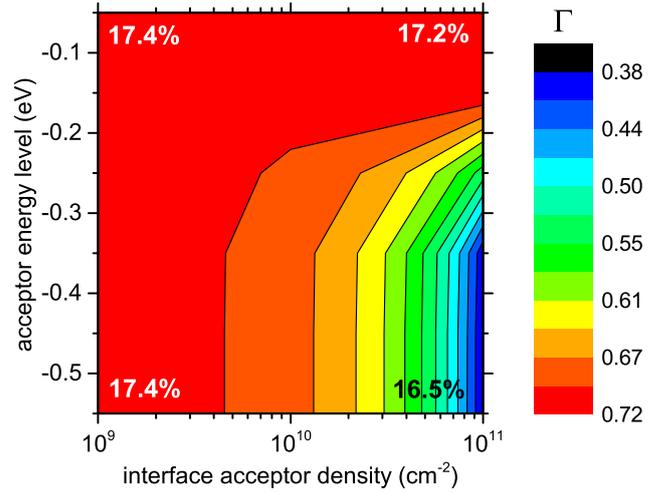

Figure 5: The effect of absorber-buffer interface acceptor density and energy level (referenced to the conduction band of the absorber layer) on the permittivity ratio sensitivity factor Γ. The overlaid numbers are the values of η_{ε_B}, i.e. the solar cell efficiency with a high buffer-to-absorber permittivity ratio, at the corresponding point in the parameter space.

4.4. Dependence on interface acceptor states

In a similar fashion, we examine in Fig. 5 the influence of an interface acceptor on Γ. If the energy level of the acceptor state is close enough to the conduction band for it to be mostly unoccupied, or if its density is too low to contribute with a appreciable amount of extra negative fixed charge, Γ is fixed to its baseline value as in the interface donor case. If the fixed negative charge provided by the acceptor becomes significant, Γ decreases without approaching a saturation value.

This simulation shows that a high $\varepsilon_n/\varepsilon_p$ ratio limits the decrease in efficiency that necessarily occurs when a high density of acceptor states in present at the heterointerface.

$V_{bi,n}/V_{bi,p}$ ratio is determined by the donor level instead of by Eq. 3, and Γ saturates to 1. At the other extreme (low donor density and low energy level), Γ approaches the baseline value of 71% shown in Fig. 2 regardless of the donor properties. This is because the amount of additional positive charge at the interface is not enough to influence the $V_{bi,n}/V_{bi,p}$ ratio significantly, which is now determined by Eq. 3 as in the baseline case.

This simulation shows that, when the Fermi level is pinned by interface donors, the $\varepsilon_n/\varepsilon_p$ ratio is irrelevant for the efficiency of the solar cell.
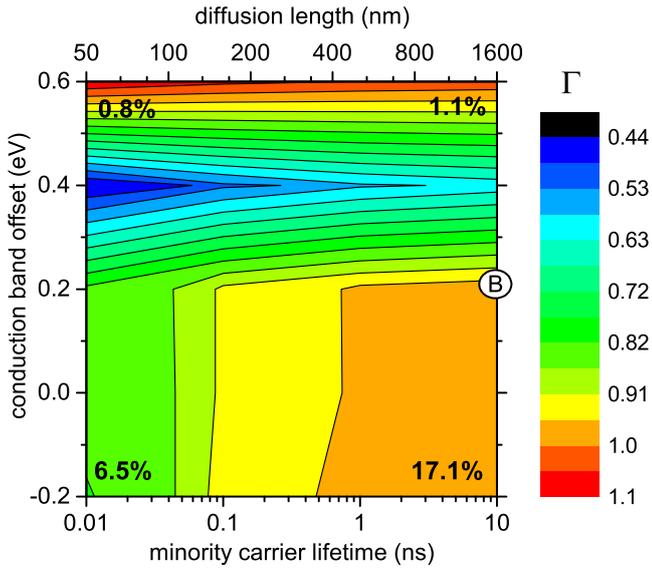
4

Figure 6: The effect of minority carrier lifetime in the absorber and conduction band offset at the absorber-buffer interface on the permittivity ratio sensitivity factor Γ. In this particular simulation, the interface recombination velocity due to neutral interface states was set to zero in order to separate effects due to depletion region widening from effects due to interface recombination. The circle with the "B" label indicates the baseline parameters. The overlaid numbers are the values of η_{ε_B}, i.e. the solar cell efficiency with a high buffer-to-absorber permittivity ratio, at the corresponding point in the parameter space.

4.5. Dependence on minority carrier lifetime and heterojunction band alignment

Finally, in Fig. 6 we show variations in Γ that are not related to the built-in voltage drop distribution, but that are instead related to variations in the depletion region width (Eq. 2 and Sec. 2.1). To exclude the effects related to the built-in voltage drop distribution (Figs. 2-5), we set the interface recombination velocity to zero, so that the $V_{bi,n}/V_{bi,p}$ ratio does not influence the efficiency, as discussed in Sec. 2.2. All other parameters are kept at their baseline value. The explored parameters are the conduction band offset and the minority carrier (electron) lifetime in the bulk of the absorber. The lifetime determines the collection depth of the photogenerated carriers out of the depletion region, with higher lifetimes giving a longer collection depth. The lifetime is inversely proportional to the density of bulk defects in the absorber N_t (Table 1), which is the parameter that has been changed in practice to obtain the range of lifetimes shown in Fig. 6. In this particular study, the variations in Γ are primarily due to short circuit current variations because changing the $\varepsilon_n/\varepsilon_p$ ratio changes the depletion region width W_p in the absorber under short circuit conditions, and therefore the total collection depth. Unless the conduction band offset is large and positive, Γ decreases as the lifetime decreases. This is in accordance with Eq. 2 because, as lifetimes decrease, a larger fraction of J_{sc} comes from carriers generated in the depletion region, hence the variation in depletion region width by variation in buffer permittivity becomes more important. Note that, even though we keep using Γ as a measure of permittivity-related effects, here it is not the permittivity ratio $\varepsilon_n/\varepsilon_p$ that causes the

observed effect but simply the permittivity of any of the two materials, according to Eq. 2. Since we keep ε_p constant in our simulation, it is ε_n alone that influences the solar cell efficiency. For a large positive conduction band offset, another mechanism limiting the short circuit current exists, i.e., the barrier to electron flow due to the conduction band spike. Electron transport through the spike depends on the kinetic energy of the electrons reaching the barrier from the absorber. This energy is, at maximum, equal to $eV_{bi,p}$ if electrons are generated outside the depletion region or at its edge. In case of generation within the depletion region, the expected value of the kinetic energy depends on the voltage drop between the point of generation and the heterojunction. That explains the drop of Γ at a conduction band offset of 0.4 eV for low lifetimes. In such a situation, most of the collected electrons come from the depletion region, so J_{sc} changes significantly due to changes in $V_{bi,p}$ by different permittivity ratios. For a spike larger that roughly 0.5 eV, all electron current from the absorber is blocked regardless of how the voltage drop is distributed and the only (few) collected electrons are from the buffer layer. Hence, Γ becomes independent of the absorber lifetimes and, in the extreme case of a 0.6 eV barrier, Γ is larger than 1 because in such conditions it is beneficial to have a *high* $V_{bi,n}/V_{bi,p}$ ratio to maximize collection efficiency *in the buffer*.

This simulation shows that a high permittivity in either the buffer or the absorber generally improves the efficiency of solar cells with short minority carrier lifetimes, even though the degree of improvement varies depending on the band alignment at the heterointerface.

5. Discussion

With the exception of this last rather unrealistic case (CBO > 0.5 eV), we note that Γ ≤ 1 in all parameter ranges explored in Figs. 2-6. Assuming that the permittivity of the absorber is fixed, this means that a high permittivity in the buffer is, in general, either beneficial or irrelevant for device performance. In state-of-the-art Cu(In,Ga)Se$_2$ solar cells it is most likely to be irrelevant. This is because high-efficiency Cu(In,Ga)Se$_2$ solar cells have sufficiently high (above 10 ns) minority carrier lifetimes, so that a high buffer permittivity is not expected to influence current collection, as explained in Sec. 2.1 and Sec. 4.5. Moreover, band gap broadening at the heterointerface and Fermi level pinning by interface donors [10, 11] are expected to lead to a low interface recombination rate and a low $V_{bi,n}/V_{bi,p}$ ratio regardless of the permittivity of the materials, as explained in Sec. 2.2 and Sec. 4.3.

On the other hand, higher band gap absorbers such as Cu(In,Ga)S$_2$, CuInS$_2$, and Cu$_2$ZnSnS$_4$ are believed to be more sensitive to interface recombination [10, 11, 15], so a high-permittivity buffer layer may be an advantage in those cases as it would decrease the $V_{bi,n}/V_{bi,p}$ ratio and increase the open circuit voltage (Sec. 2.2 and Sec. 4.2). In the case of Cu$_2$ZnSnS$_4$ and Cu$_2$ZnSnSe$_4$, the minority carrier lifetimes appear to be significantly lower than in Cu(In,Ga)Se$_2$ [16]. Hence, with such absorbers, a high buffer permittivity may also be beneficial for current collection by widening the depletion region (Sec. 2.1

and Sec. 4.5). Note that, the lower the permittivity of the absorber, the easier it is to obtain a high $\varepsilon_n/\varepsilon_p$ ratio by different buffer materials. This means that finding a high-permittivity buffer material is a less stringent requirement in solar cells based on low-permittivity absorbers.

6. Conclusion

When designing novel absorber-buffer-window combinations for heterojunction solar cells, it is advantageous to choose among high-permittivity buffer materials. This is because a high buffer-to-absorber permittivity ratio makes a solar cell more robust against non-idealities that may be encountered in early stage research, such as low buffer doping, large required buffer thickness, suboptimal band alignment, interface recombination, and negative interface charge. Even among existing heterojuction solar cell technologies, those that are limited by interface recombination may experience an improvement in open circuit voltage if a high-permittivity buffer material is used. Many oxide materials have a high permittivity, in addition to other desirable properties such as high band gaps and natural n-type doping. Hence, they may be the preferred class of materials as buffer layers for p-type absorbers and have already been used with promising results [17–19]. A high permittivity in either the buffer or the absorber also improves current collection when minority carrier lifetimes are low. Therefore, while there is a clear design rule for the permittivity of the buffer layer, there is not a universal design rule for the permittivity of the absorber layer.

Acknowledgments

References

[1] M. A. Green, K. Emery, Y. Hishikawa, W. Warta, E. D. Dunlop, Solar cell efficiency tables (version 48), Progress in Photovoltaics: Research and Applications 24 (7) (2016) 905–913. doi:10.1002/pip.2788.

[2] N. Naghavi, D. Abou-Ras, N. Allsop, N. Barreau, S. Bücheler, A. Ennaoui, C.-H. Fischer, C. Guillen, D. Hariskos, J. Herrero, R. Klenk, K. Kushiya, D. Lincot, R. Menner, T. Nakada, C. Platzer-Björkman, S. Spiering, A. Tiwari, T. Törndahl, Buffer layers and transparent conducting oxides for chalcopyrite Cu(In,Ga)(S,Se)$_2$ based thin film photovoltaics: present status and current developments, Progress in Photovoltaics: Research and Applications 18 (6) (2010) 411–433. doi:10.1002/pip.955.

[3] S. Sze, K. K. Ng, Physics of semiconductor devices, Wiley, 2004, p. 126.

[4] A. Crovetto, A. Cazzaniga, R. B. Ettlinger, J. Schou, O. Hansen, Optical properties and surface characterization of pulsed laser-deposited Cu$_2$ZnSnS$_4$ by spectroscopic ellipsometry, Thin Solid Films 582 (2015) 203–207. doi:10.1016/j.tsf.2014.11.075.

[5] A. Crovetto, R. Chen, R. B. Ettlinger, A. C. Cazzaniga, J. Schou, C. Persson, O. Hansen, Dielectric function and double absorption onset of monoclinic Cu$_2$SnS$_3$: Origin of experimental features explained by first-principles calculations, Solar Energy Materials and Solar Cells 154 (2016) 121–129. doi:10.1016/j.solmat.2016.04.028.

[6] R. Scheer, H.-W. Schock, Chalcogenide Photovoltaics, Wiley-VCH Verlag GmbH & Co. KGaA, Weinheim, Germany, 2011, pp. 137–139, p. 315, p. 320. doi:10.1002/9783527633708.

[7] O. V. Tereshchenko, F. J. K. Buesink, F. B. J. Leferink, An overview of the techniques for measuring the dielectric properties of materials, in: 2011 XXXth URSI General Assembly and Scientific Symposium, IEEE, 2011, pp. 1–4. doi:10.1109/URSIGASS.2011.6050287.

[8] M. Burgelman, P. Nollet, S. Degrave, Modelling polycrystalline semiconductor solar cells, Thin Solid Films 361-362 (2000) 527–532. doi:10.1016/S0040-6090(99)00825-1.

[9] M. Gloeckler, Device physics of Cu(In,Ga)Se$_2$ thin-film solar cells, Ph.D. thesis, Colorado State University (2005), p. 31, p. 56.

[10] W. N. Shafarman, S. Siebentritt, L. Stolt, Cu(InGa)Se$_2$ Solar Cells, in: A. Luque, S. Hegedus (Eds.), Handbook of Photovoltaic Science and Engineering, John Wiley & Sons, Ltd, Chichester, UK, 2011, Ch. 13, pp. 575–578, pp. 580–581.. doi:10.1002/9780470974704.

[11] R. Klenk, Characterisation and modelling of chalcopyrite solar cells, Thin Solid Films 387 (1-2) (2001) 135–140. doi:10.1016/S0040-6090(00)01736-3.

[12] P. Li, R. Anderson, R. Plovnick, Dielectric constant of CuInSe$_2$ by capacitance measurements, Journal of Physics and Chemistry of Solids 40 (4) (1979) 333–334. doi:10.1016/0022-3697(79)90113-6.

[13] G. A. Samara, Temperature and pressure dependences of the dielectric constants of semiconductors, Physical Review B 27 (6) (1983) 3494–3505. doi:10.1103/PhysRevB.27.3494.

[14] H. Finkenrath, N. Uhle, Der einfluss der gitterschwingungen auf die ultrarot-reflexion von CdO, Solid State Communications 5 (11) (1967) 875–877. doi:10.1016/0038-1098(67)90319-5.

[15] O. Gunawan, T. K. Todorov, D. B. Mitzi, Loss mechanisms in hydrazine-processed Cu$_2$ZnSn(Se,S)$_4$ solar cells, Applied Physics Letters 97 (23) (2010) 233506. doi:10.1063/1.3522884.

[16] I. L. Repins, H. Moutinho, S. G. Choi, A. Kanevce, D. Kuciauskas, P. Dippo, C. L. Beall, J. Carapella, C. DeHart, B. Huang, S. H. Wei, Indications of short minority-carrier lifetime in kesterite solar cells, Journal of Applied Physics 114 (8) (2013) 084507. doi:10.1063/1.4819849.

[17] A. Crovetto, C. Yan, B. Iandolo, F. Zhou, J. Stride, J. Schou, X. Hao, O. Hansen, Lattice-matched Cu$_2$ZnSnS$_4$/CeO$_2$ solar cell with open circuit voltage boost, Applied Physics Letters 109 (23) (2016) 233904. doi:10.1063/1.4971779.

[18] C. Platzer-Björkman, C. Frisk, J. K. Larsen, T. Ericson, S.-Y. Li, J. J. S. Scragg, J. Keller, F. Larsson, T. Törndahl, Reduced interface recombination in Cu$_2$ZnSnS$_4$ solar cells with atomic layer deposition Zn$_{1-x}$Sn$_x$O$_y$ buffer layers, Applied Physics Letters 107 (24) (2015) 243904. doi:10.1063/1.4937998.

[19] W. Hsu, C. M. Sutter-Fella, M. Hettick, L. Cheng, S. Chan, Y. Chen, Y. Zeng, M. Zheng, H.-P. Wang, C.-C. Chiang, A. Javey, Electron-Selective TiO$_2$ Contact for Cu(In,Ga)Se$_2$ Solar Cells, Scientific Reports 5 (2015) 16028. doi:10.1038/srep16028.

A. Contact properties		Front	Back
S_e (cm/s)		10^7	10^7
S_h (cm/s)		10^7	10^7
Optical properties		Transmission = 1	Mo
ϕ_{Bn0}, ϕ_{Bp0} (eV)		0	0
B. Layer properties	**Window**	**Buffer**	**Absorber**
Thickness (nm)	50	100	2500
E_g (eV)	3.3	2.4	1.15
χ (eV)	4.5	4.3	4.5
ε_r	9.0	10.0	13.6
N_C (cm^{-3})	2.2×10^{18}	2.2×10^{18}	6.7×10^{17}
N_V (cm^{-3})	1.8×10^{19}	1.8×10^{19}	1.5×10^{19}
μ_e (cm^2/Vs)	100	100	100
μ_h (cm^2/Vs)	25	25	10
$N_{d/a}$ (cm^{-3})	$N_d = 1 \times 10^{18}$	$N_d = 1 \times 10^{16}$	$N_a = 1 \times 10^{16}$
C. Defect states	**Window**	**Buffer**	**Absorber**
Type	N.A.	Neutral	Neutral
Energy distribution		Single level	Single level
N_t (cm^{-3})		2×10^{17}	2×10^{13}
E_t (eV)		$E_V + 1.2$	$E_V + 0.8$
σ_e (cm^2)		10^{-13}	5×10^{-13}
σ_h (cm^2)		10^{-13}	1×10^{-15}
D. Interface defect	**Buffer/Window**	**Absorber/Buffer**	
Type	N.A.	Neutral	
Energy distribution		Single level	
E_t (eV)		$E_{V,CIGS} + 0.6$	
N_t (cm^{-3})		10^{14}	
σ_e, σ_h (cm^2)		10^{-16}	

Table 1: The baseline parameters used for simulating the absorber/buffer/window heterojunction solar cell analyzed in this work. The materials parameters for each layer are taken from CIGS (absorber), CdS (buffer), and ZnO (window) following various literature sources [6, 9, 10]. S_e and S_h are the interface recombination velocities for electrons and holes; ϕ_{Bn0} and ϕ_{Bp0} are the contact barrier heights; E_g is the band gap; χ is the electron affinity; ε_r is the static relative permittivity; N_C and N_V are the effective density of states in the conduction and valence band respectively; they are derived from the effective masses of electrons and holes, which are taken as $0.09 m_0$ and $0.7 m_0$ respectively (m_0 is the electron rest mass); μ_e and μ_h are the electron and hole mobilities; $N_{d/a}$ is the shallow dopant density in the case of donors and acceptors, respectively; N_t is the defect density; E_t is the defect energy level (referenced to the valence band maximum E_V of the material); σ_e and σ_h are the capture cross sections for electrons and holes respectively. In the simulation, the conduction band offsets (CBO) between layers are determined by the difference in their electron affinity. Hence, the baseline CBO at the absorber/buffer (buffer/window) interface is +0.2 eV (−0.2 eV).